34th AIAA Fluid Dynamics Conference 28 June - 1 July, 2004 / Portland, Oregon

STS-107 Investigation Ascent CFD Support

Reynaldo J. Gomez* and **Darby Vicker***
NASA Johnson Space Center
Houston, Texas

Stuart E. Rogers†, **Michael J. Aftosmis**‡, and **William M. Chan**§
NASA Ames Research Center
Moffett Field, California

Robert Meakin¶
US Army AFDD (AMCOM)
Moffett Field, California

Scott Murman‖
ELORET
Moffett Field, California

This paper provides an overview of the computational fluid dynamics analysis of the ascent of the Space Shuttle Launch Vehicle during the investigation of the STS-107 accident. The analysis included both steady-state and unsteady calculations performed with the Overflow and Cart3D flow solvers. The unsteady calculations include moving body, six degree-of-freedom simulations of foam debris shed from the region of the left bipod-ramp of the vehicle. Many such debris trajectories were computed, some of which impacted the vehicle. The analysis provided an estimate of the speed at which such a piece of debris would strike the wing leading edge of the Shuttle Orbiter. These results were supplied to the Columbia Accident Investigation Board, and guided the choice of the impact velocity and foam size selected for the foam-firing test done as part of the investigation. This testing subsequently showed that it was possible for a piece of foam debris to cause massive damage to the Shuttle Orbiter wing Reinforced-Carbon-Carbon panels and T-seals, creating a breach where hot gases could enter the wing structure during reentry.

I. Introduction

On January 16th 2003, the Space Shuttle Columbia began its last mission, designated STS-107. During the ascent, a piece of foam insulation was shed from the external tank and struck the leading edge of the left wing of the Orbiter. Although it was not known at the time, this foam-debris strike caused enough damage to the wing that Columbia was lost during reentry on February 1st, 2003.[1] Despite the fact that the debris event was captured on film, there was significant ambiguity as to the size and speed of the debris. The need to determine the possible size, speed, and impact location of the debris led NASA and the Columbia Accident Investigation Board (CAIB) to utilize Computational Fluid Dynamics (CFD) techniques to analyze

*Aerospace Engineer. Member AIAA.
†Aerospace Engineer. Associate Fellow AIAA.
‡Research Scientist. Senior Member AIAA.
§Computer Scientist. Senior Member AIAA.
¶Senior Staff Scientist. Senior Member AIAA.
‖Senior Research Scientist. Member AIAA.
This material is declared a work of the U.S. Government and is not subject to copyright protection in the United States.

the event. In addition to simulations of the debris, the investigation considered the aerodynamic forces acting on the foam bipod ramp, and the detailed flow physics during ascent as it searched for clues to the root cause of the foam shedding.

This analysis utilized the Overflow,[2,3] Overflow-D[4,5] and Cart3D[6,7] simulation tools. Steady-state Overflow calculations were performed at several flight conditions of the Columbia ascent. These solutions were used not only to investigate the aerodynamic forces on the vehicle, but also to provide a flowfield for the ballistic integration of possible flight paths of debris pieces. This ballistic integration ignores the effect that the traveling debris has on the surrounding flowfield, and it assumes that the only aerodynamic force on the debris is the drag force acting in the direction of the local relative wind vector. Significantly more accurate and more expensive calculations were also used; these were unsteady, moving-body, CFD simulations of the entire flowfield with proper modeling of the aerodynamic forces and moments acting on the debris. The debris was allowed six degrees of freedom (6-DOF) of movement in response to these forces and moments. The 6-DOF simulations are capable of showing the effect of the specific debris shape on its trajectory as well as the effect of the debris on the vehicle's flowfield.

This paper provides an overview of the ascent CFD work performed at the Johnson Space Center and at Ames Research Center during the investigation of the STS-107 accident. The following sections include a description of the CFD tools used, including the grid-generation, flow solvers, and computer resources. Following this is a summary of the CFD results that were obtained, both steady-state and unsteady calculations. All of the results of this work was provided to the CAIB during the investigation, and was included in an appendix of the final CAIB report.[8]

II. History of Shuttle Overflow CFD

The Overflow[2,3] code and the chimera grid approach[9] has been in use to solve the flow over the integrated Space Shuttle Launch Vehicle (SSLV) for over 16 years. Buning *et al*[10] first reported results using this approach in 1988, and using grid sizes up to 750,000 points, obtained reasonably good comparison with wind-tunnel pressure coefficient (Cp) data. The geometry in their computations consisted solely of the right half of the vehicle, and included simplified versions of the Orbiter, the right Solid-Rocket Booster (SRB), and the External Tank (ET). Over the next several years, this computational model was refined and continued to be used to study the SSLV ascent flow field, see Pearce *et al.*[11] Slotnick *et al*[12] used this approach to simulate the SRB plumes, including variable-gamma effects. By 1994, the procedure was refined to include more geometric detail, and utilized 113 grids and 16 million grid points; see Slotnick *et al,*[13] Gomez and Ma,[14] and Martin *et al.*[15]

III. Tools

This section briefly describes the CFD tools and computational resources used in the current work.

A. Overflow

The Overflow[2,3] code solves the Navier-Stokes equations using a finite-difference formulation in body-fitted curvilinear meshes. The calculations were run using central differencing of the inviscid and the viscous fluxes, and a diagonalized, approximate-factorization, implicit solver. The Spalart-Allmaras turbulence model was selected. The code was started from initial conditions using full-multi-grid sequencing on three levels, and was run to steady-state convergence using three-level multi-grid acceleration. The code was executed on an SGI Origin 3000 shared-memory architecture computer, and utilized a multi-level parallelism[16] (MLP) algorithm. The MLP code uses native UNIX directives, and two levels of parallelism. The coarse-grained parallelism consists of splitting the flow solution into groups of zones, such that each group contains nearly the same number of grid points. On the fine-grained level, each group is assigned a number of CPUs. These CPUs execute the code's "do" loops in parallel. The performance of the MLP version of Overflow has been

shown to scale linearly with increasing number of CPUs beyond 512 CPUs for large problems. Most of the current Overflow calculations used a total of 128 CPUs and 24 groups.

B. Overflow-D

The Overflow-D[4,5] code is based on version 1.6au of the NASA standard Overflow, but has been significantly enhanced to accommodate moving body applications. The Overflow-D enhancements include the following capabilities: on-the-fly generation of off-body grid systems; MPI enabled scalable parallel computing; automatic load balancing; aerodynamic force and moment computations; general 6-DOF model; rigid-body relative motion between an arbitrary number of bodies; domain connectivity; solution error estimation; and grid adaptation in response to body motion and/or estimates of solution error.

Overflow-D employs the "near-body" and "off-body" domain partitioning method described in Refs. 4 and 5; these are used here as the basis of discretization of the SSLV. In the approach, the near-body portion of a domain is defined to include the surface geometry of all bodies being considered and the volume of space extending a short distance away from the respective surfaces. The construction of near-body grids and associated inter-grid connectivity is a classical Chimera-style[9] decomposition of the near-body domain. It is assumed that near-body grids provide grid-point distributions of sufficient density to accurately resolve the flow physics of interest (i.e., boundary-layers, vortices, etc.) without the need for refinement. This is a reasonable constraint since near-body grids are only required to extend a short distance away from body surfaces.

The off-body portion of the domain is defined to encompass the near-body domain and extend out to the far-field boundaries of the problem. The off-body domain is filled with overlapping uniform Cartesian grids of variable levels of refinement. The off-body grid resolution amplification factor between successive levels is 2. The near-body plus off-body partitioning approach facilitates grid adaptation in response to proximity of body components and/or to estimates of solution error within the topologically simple off-body grid system.

C. Cart3D

The Cart3D[6,7] package solves the Euler equations using a finite-volume formulation on unstructured Cartesian meshes. Mesh generation with Cart3D is fully automated. The package takes as input the triangulated surface geometry and generates an unstructured Cartesian volume mesh by subdividing the computational domain based upon the geometry, and any pre-specified regions of mesh refinement. In this manner, the space near regions of high surface curvature contains highly-refined cells, while areas away from geometry and pre-specified regions contain coarser cells. The intersection of the solid geometry with the regular Cartesian hexahedra is computed, and polyhedral cells are formed which contain the swatch of surface geometry covered by the Cartesian hexahedra. Cells interior to the geometry are automatically removed. The solid-wall boundary conditions for the flow solver are then specified within these "cut-cell" polyhedra. The volume meshing procedure is robust,[6] and does not require user intervention. The meshing scheme is extremely fast (over 1 million cells-per-minute) and meshes are usually created on-demand in the run script and not stored after the computation has completed. Cart3D's solver is based on an explicit multi-stage procedure with multigrid acceleration. Convergence of this solver is comparable with the fastest multigrid solvers in the literature.[7] Cart3D is parallelized using a domain decomposition strategy based upon the use of space-filling curves. This approach leads to excellent scalability using either OpenMP[7] or MPI[17] for communication on distributed and shared memory computers.[18] Prototypes of the moving-body enhancements and 6-DOF module used in Cart3D were presented in 2002 and 2003.[19–21]

D. Computational Resources

Nearly all of the calculations presented in the current work were performed on a 1024-CPU SGI Origin 3000 at the NASA Advanced Supercomputer (NAS) facility at Ames Research Center. Due to the urgency of these calculations, these jobs were run in a special high-priority batch queue permitting continuous running

and resulting in a very rapid turn-around of the results. This, combined with the gigabit ethernet connection from the Origin to a group of workstations and the excellent support from the NAS staff, resulted in an ideal computing environment for this investigation. Additional computing time for the initial Overflow-D calculations was provided by the U.S. Army Research Laboratory Major Shared Resource Center.

IV. Geometry and Grid Generation

Figure 1 shows a view of the entire Space Shuttle Launch Vehicle (SSLV). The computational models in the current work included all of the main components of the SSLV, including the Orbiter, the ET, and the SRBs. Also included were the major attach hardware between the components, and most importantly, the left foam bipod ramp which was the source of the foam debris. The details of the overset and Cartesian grids are given in the following two subsections.

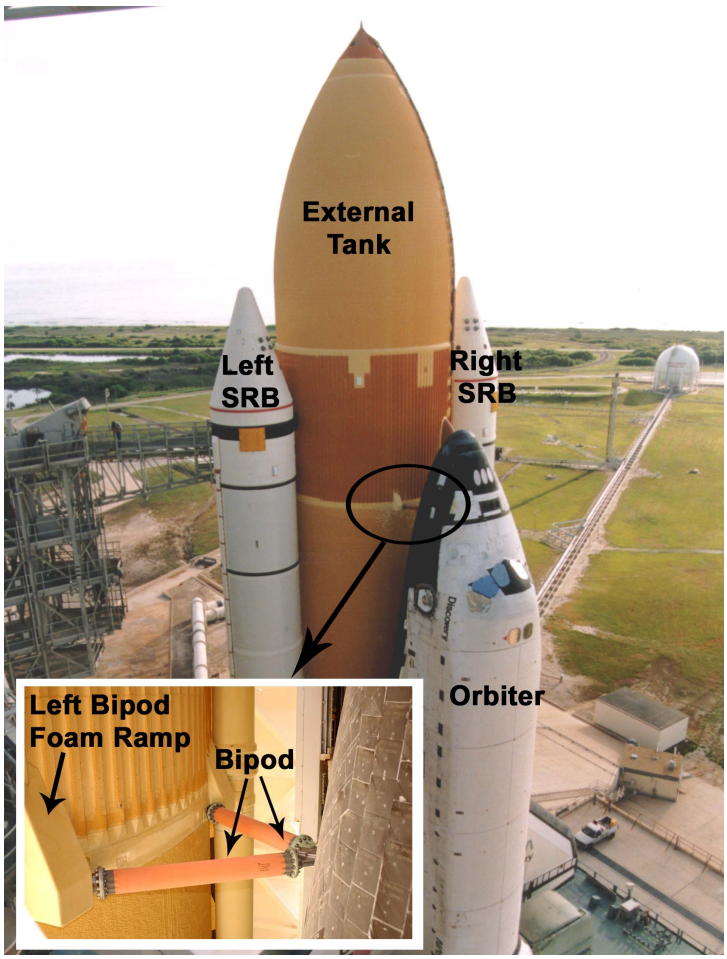


Figure 1. Photo of the SSLV and the foam bipod ramp.

A. Overset Grid Generation

The current investigation work began by updating the Shuttle ascent overset grid generation to include several new features and to provide automation of the solution process. These upgrades to the overset-grid generation had begun before 2003, but were accelerated shortly after the STS-107 accident in order to provide the needed capability for the current work. The new capabilities included a number of improvements to the geometry and the overset grid topologies. One such improvement was the ability to deflect automatically the four Orbiter elevons and the body flap to any desired operational angle and build high-fidelity surface grids around the resulting geometry. This was accomplished using a series of scripts and programs which can reliably produce usable grids for any combination of deflection of these control surfaces, an example of which is shown in figure 2. Another improvement was the refinement of the grids around the left-bipod strut and ramp. Previous to the STS-107 investigation, the grids covering this area were quite coarse and most of the geometric detail was omitted. As part of the the current work, this area was greatly refined in an effort to compute the aerodynamic forces acting on the bipod ramp. Figure 3 shows a close-up of the resulting grids on the left bipod strut and ramp. The maximum surface-grid spacing on the bipod ramp is 1.6 inches.

Another major improvement to the grid-generation process was the implementation of the Chimera Grid Tools (CGT)[22,23] scripting system. This provided an easy method of configuration control, the ability

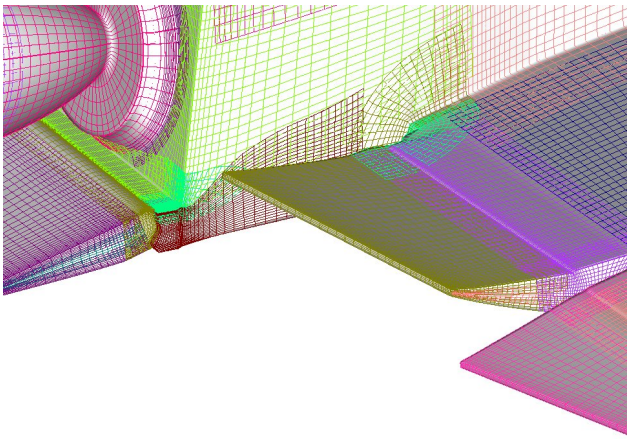


Figure 2. Control-surface geometry and grids.

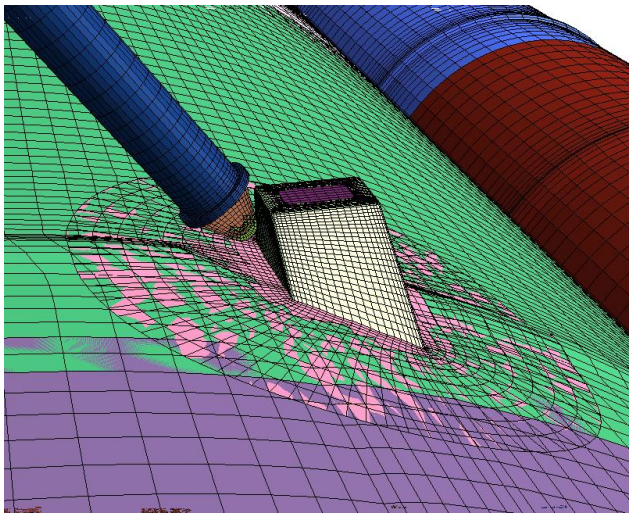


Figure 3. Overset surface grids on the left bipod ramp.

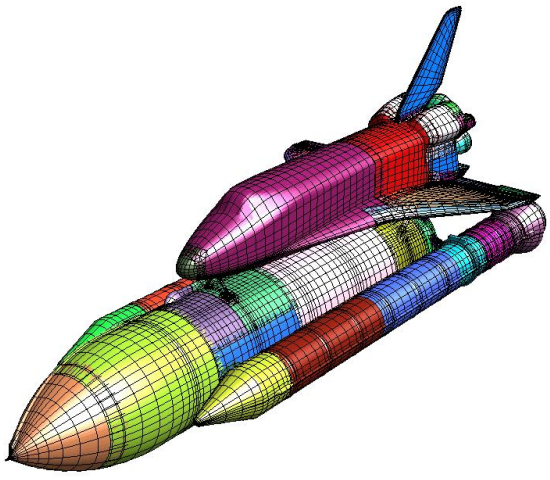


Figure 4. Overset surface grids on entire ascent vehicle.

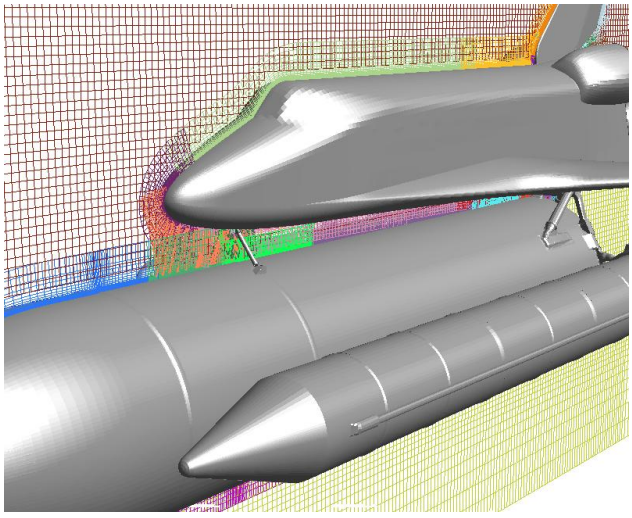


Figure 5. Overset grids in the center plane.

to automate the building of the volume grids, and the ability to automatically generate the necessary input files for all of the software programs used in the grid pre-processing, the running of the Overflow solver, and the final post-processing. The CGT scripts are written using the Tcl scripting language. The current implementation includes the ability to select specific vehicle configurations with or without certain components such as the SRB, the ET, and various attach hardware. Once the configuration has been selected and the volume grids are generated, the individual grids are connected using the Pegasus5 software.[24]

A view of the surface grids on the entire ascent vehicle configuration is shown in figure 4, which plots every fourth grid line in each direction for clarity. The typical surface-grid spacing is approximately four inches. The wall-normal spacing of all of the volume grids is 1.6×10^{-4} inches. The complete grid system for this configuration is composed of 167 zones and just over 24 million grid points. A view of the grids in the center plane of the vehicle is shown in figure 5.

V. Cartesian Grid Generation

As described in Ref. 6, the Cartesian-mesh generation system in Cart3D takes a series of closed (watertight) triangulations as input and automatically produces a non-body-fitted Cartesian mesh which is locally refined to resolve surface curvature. Each piece of input geometry is a "component" of the full configuration. In the case of the STS-107 ascent geometry, these included components for the ET, the SRBs, various components making up the Columbia Orbiter, and several components for the attach hardware. In all, the launch configuration was made up of 38 components described by about 550,000 triangles. The attach hardware includes the aft-attach hardware, and more importantly the forward bipod and the two bipod ramps.

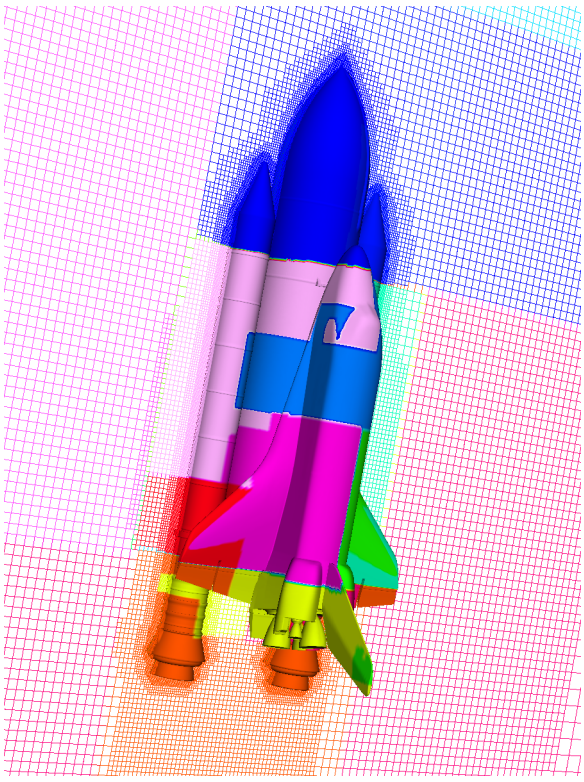


Figure 6. Cartesian mesh with 4.5 million cells showing mesh partitioning into 16 subdomains.

Figure 6 shows a view of a typical Cartesian mesh used for the simulations. This particular mesh is from simulations performed on day six of the investigation, and more detail of the geometry was added as the investigation progressed. Mesh refinement in response to surface detail is obvious in this figure. In addition, the mesh has a pre-specified adaptation region covering the entire geometry and smaller ones near the forward attach hardware (bipod and bipod ramps). When simulations are run on parallel computers, Cart3D uses a domain-decomposition technique to distribute the work among the various processors.[7] The coloring of the mesh and surface in figure 6 shows this partitioning for a 16 processor system.

The mesh shown has approximately 4.5 million cells, at 15 levels of refinement. Nominal resolution near the vehicle was approximately four feet and the region between the Orbiter and external tank was resolved with a background resolution of approximately one foot. The pre-specified refinement region near the forward attach hardware used about 1.5 inch resolution to cover the bipod and bipod ramp. As the bipod ramp debris moves during the 6-DOF moving-body simulations, the mesh responds not only by re-adapting to the ramp in its new position, but also by moving the pre-specified refinement region that covers the space near the moving bipod ramp. In this manner the mesh resolution tracks the debris over its trajectory through the flow field.[21] The mesh partitioning shown in figure 6 is similarly adjusted at each time step to maintain

load balance as the mesh and geometry evolve.

VI. Steady-State Solutions

Steady-state Overflow and Cart3D calculations were performed for a number of flight conditions experienced along the STS-107 ascent trajectory. The Mach numbers of these conditions ranged from 0.6 to 4.0, and included the maximum dynamic pressure condition at Mach = 1.25, and the conditions at a mission elapsed time (MET) of 81.7 seconds. This is the MET when the bipod-ramp foam was seen to shed from the ET and fly back and impact the left wing of the Orbiter. This occurred at an altitude of 65,820 feet, traveling at Mach = 2.46 and a velocity of 2324 feet/sec. Each steady-state Overflow run required about 1000 SGI Origin CPU hours.

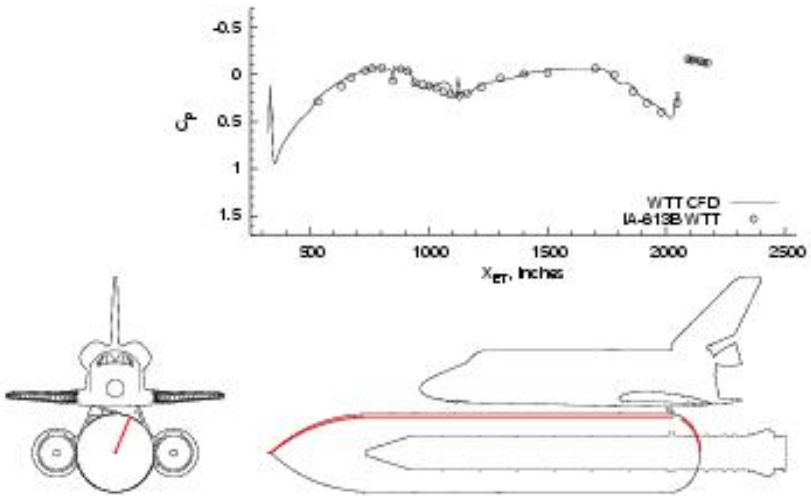


Figure 7. *Cp* **comparison at Phi = 157.5 deg.**

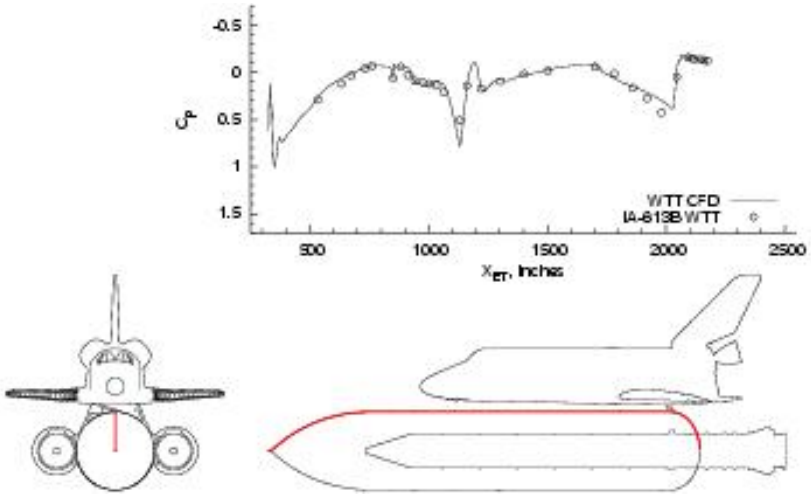


Figure 8. *Cp* **comparison at Phi = 180.0 deg.**

A. Validation

In order to validate the current CFD results, extensive comparisons of (Cp) between Overflow calculations and existing experimental and flight data have been made. These include comparisons of integrated forces and moments, and of Cp data covering the Orbiter, ET, and SRB components. A presentation of all of this data is beyond the scope of this paper. In general, very good agreement is seen between the experimental and computational results. Plots of the Cp comparisons are presented here on two axial rows on the ET at circumferential angles of 157.5 deg and 180 deg, as illustrated in figures 7 and 8. The experimental Cp is plotted with a circle and the CFD results are drawn with a solid line. The experimental data comes from the Space Shuttle Program test number IA-613.[25] The comparison is made for a Mach number of 2.50, a Reynolds Number per full-scale inch of 6250, an angle of attack of 2.03 deg, and a zero slide-slip angle. These results show that the CFD is in good agreement with the experimental data.

B. Cart3D and Overflow Comparisons

The following three figures show a comparison of the surface *Cp* data generated by both Cart3D and Overflow steady-state solutions. In each of these three figures, the Cart3D *Cp* is plotted on the left, the Overflow data is plotted on the right, and the difference between the two is shown in the middle. In the color contours in the middle plots, white represents zero difference between the two; red represents higher pressure in the Cart3D solution, and blue represents higher pressure in the Overflow solution. The upper half of each of these figures shows the forward third of the ET and SRB surfaces, whereas the lower half shows a closer view of the bipod region of the ET. Figure 9 shows the solutions at a Mach number of 0.6. Mach numbers of 1.06 and 2.46 are plotted in figures 10 and 11, respectively. Overall the flow solvers show very similar flow structure and evidence of shocks in the flow at about the same locations. The effect of the viscosity in the Overflow solutions is seen as the foot-prints of the shocks on the surface *Cp* are much crisper in the Cart3D solutions. Differences due to viscosity increase as the boundary layer gets thicker with increasing altitude. At 65,820 feet the Mach=2.46 solutions show the largest local differences: the Overflow solution has a significant amount of flow-separation occurring on the ET surface just upstream of the bipod region. This is due to both a thicker boundary layer and the intersection of the SRB nose shocks with the Orbiter-nose shock just upstream of the bipod region. This separation results in a dramatically different shock pattern, and large differences in the local flow solutions. The viscous Overflow results provide a better representation of the actual flow in this vicinity and so the Overflow computations are used to estimate the actual bipod-ramp aerodynamic loads in the following section.

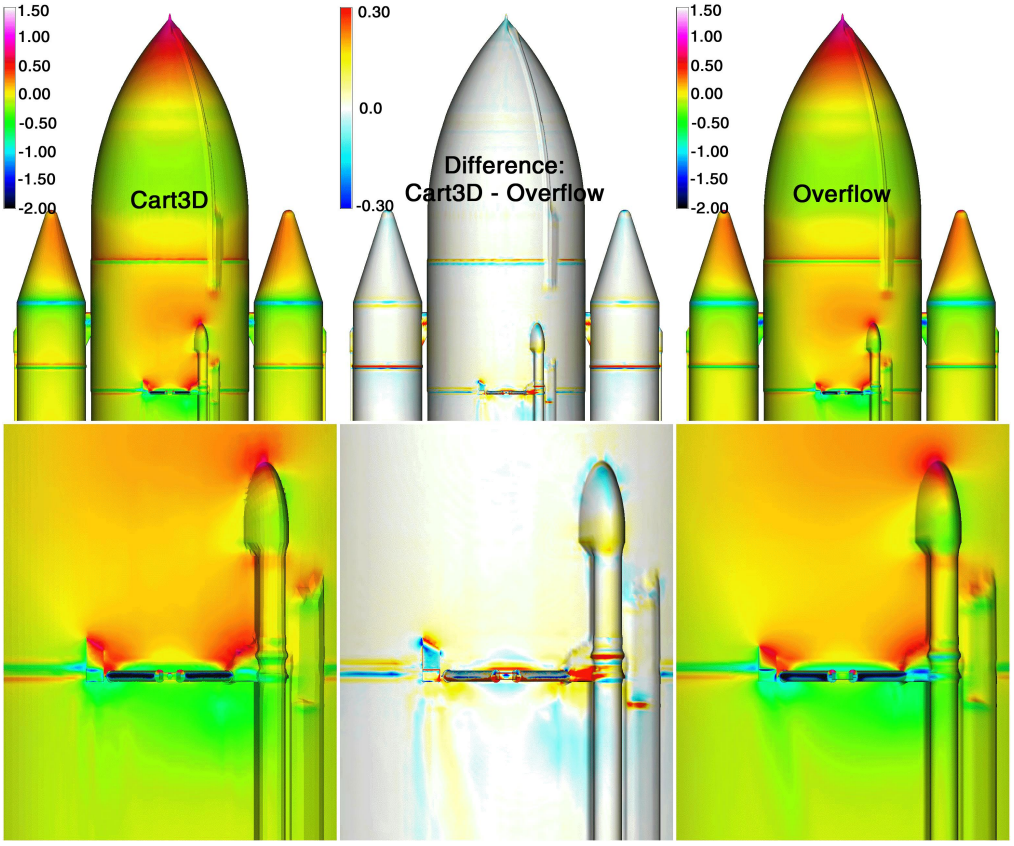


Figure 9. Comparison of Cart3D and Overflow *Cp* at Mach = 0.6, Alpha = -1.7 deg, Beta = -0.88 deg.

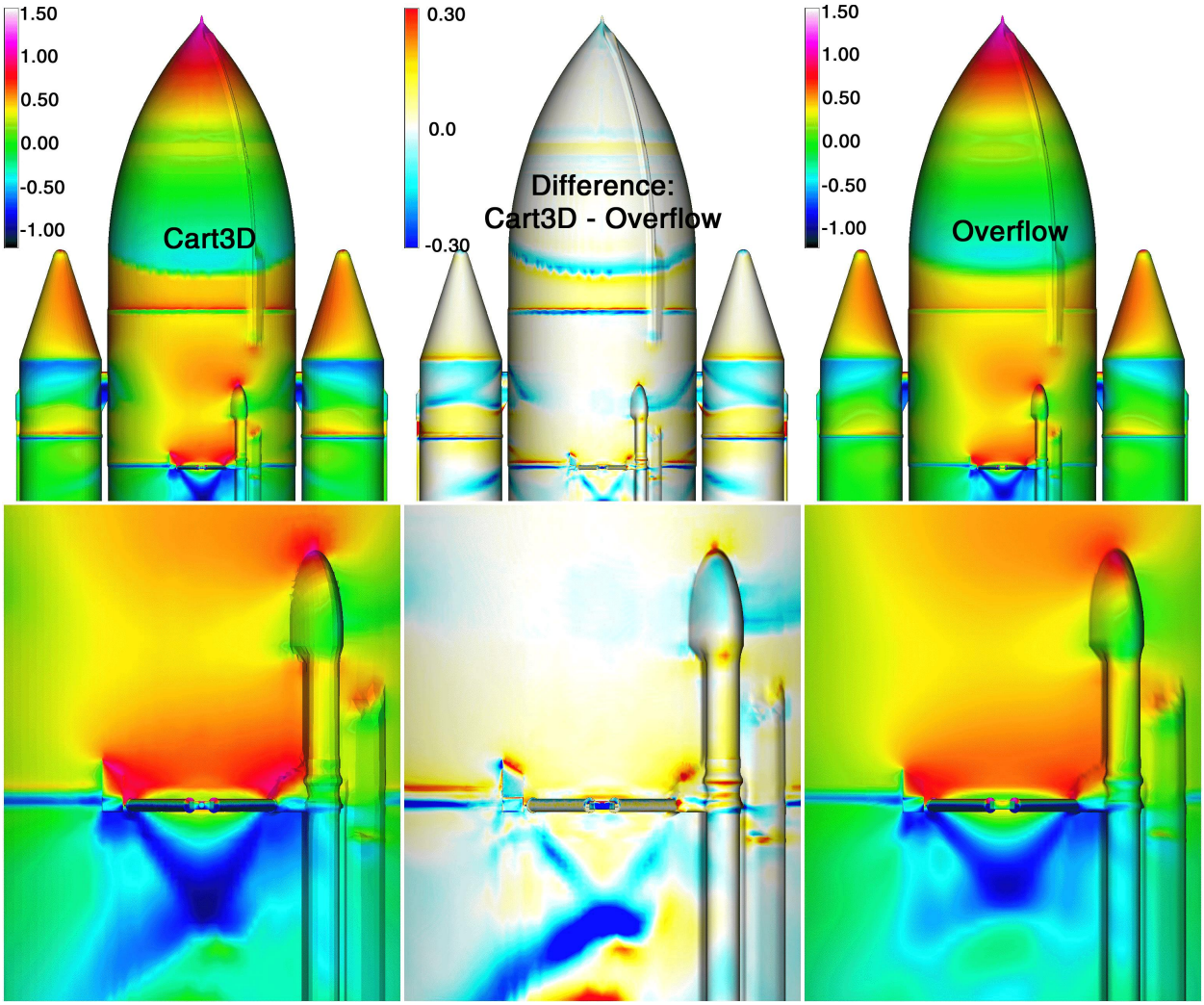


Figure 10. Comparison of Cart3D and Overflow Cp at Mach = 1.06, Alpha = -3.9 deg, Beta = -0.8 deg.

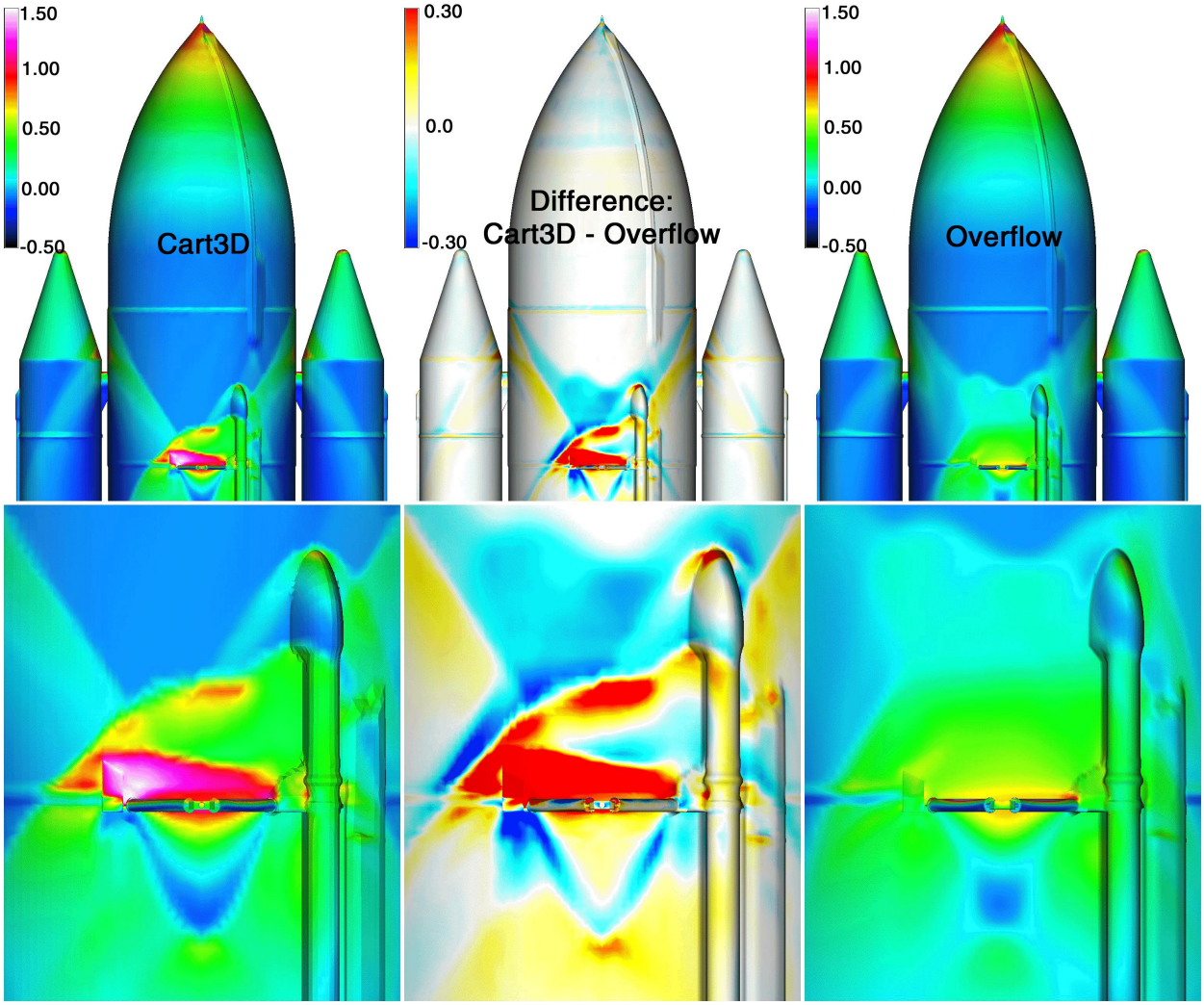


Figure 11. Comparison of Cart3D and Overflow Cp at Mach = 2.46, Alpha = 2.08 deg, Beta = -0.09 deg.

C. Bipod-Ramp loads

A key concern of the investigation was whether external air loads caused or contributed to the failure of the foam ramp resulting in the debris release. Bipod ramp airloads were evaluated using the Overflow steady-state flow solutions at several Mach numbers. These CFD loads were compared to design certification loads and to air loads at STS-107 conditions predicted using the engineering techniques used to design the bipod ramps. The engineering results consistently bounded the CFD analysis indicating that the design certification loads were conservative and did not under predict the actual load environments. These comparisons are shown in figures 12, 13, and 14. The design requirement curve is based on a high-dynamic pressure trajectory designed to fly at the Shuttle structural design limits. The curves from the engineering loads at the STS-107 conditions were derived from the same analysis procedure, but using the STS-107 trajectory dynamic pressures to compute the various loads. The CFD symbols are the loads computed from the current Overflow steady-state simulations. The axial force plotted in figure 12 is the force acting in the zero-incidence flow direction; the radial force plotted in figure 13 is the force acting inward toward the centerline of the ET; and the side force plotted in figure 14 is the force acting tangentially to the ET surface to the left-wing side of the vehicle. Thus it can be seen that the loads computed by Overflow are bounded by the design loads throughout the trajectory, and that the steady aerodynamic loads alone do not explain why the bipod ramp broke loose during the flight.

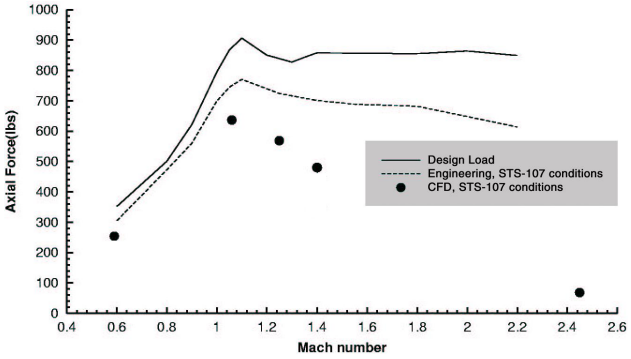


Figure 12. Left bipod ramp axial force versus Mach number.

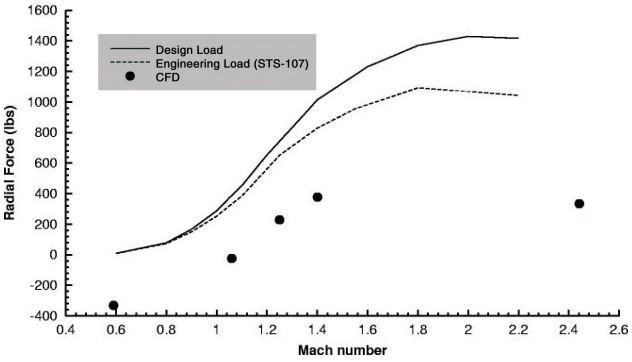


Figure 13. Left bipod ramp radial force versus Mach number.

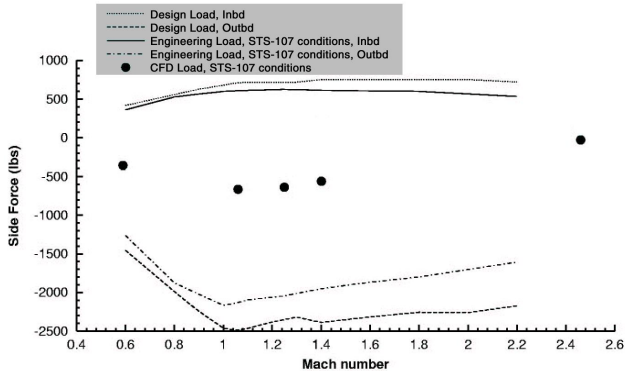


Figure 14. Left bipod ramp side force versus Mach number.

VII. 6-DOF Unsteady Solutions

Over 40 Overflow-D and over 400 Cart3D 6-DOF simulations were run during the investigation. Each of the Cart3D cases required approximately 1000 CPU hours on an SGI Origin 3000 computer. Typically these cases were run using 64 CPUs in parallel, and thus required approximately 16 hours of wall-clock time. The Overflow-D cases required at least 20 times more CPU time than the Cart3D simulations. All of these cases were run with the conditions at MET=81.7 seconds, and neglected the acceleration of the vehicle. These runs included parametric studies on the effect of time-step size and on the grid resolution needed for these debris cases. Six differ-

ent specific debris shapes and sizes were simulated, based on the several possible foam-shedding scenarios. These ranged from 167 cubic inches in volume to 1450 cubic inches. Four of these debris pieces are shown in figure 15. For each of these debris shapes, various initial velocity and rotation conditions were applied to the debris. The debris path was very sensitive to these initial conditions: some combinations of conditions caused the debris to fly well above and outboard of the wing. Others caused the debris to fly under the wing, or to hit somewhere along the fuselage.

One significant finding of the 6-DOF calculations was that the axial velocity of the debris relative to the vehicle was nearly independent of the debris initial conditions. Instead, it was primarily dependent on the mass of the debris. This is illustrated in figure 16 which plots the Cart3D computed debris axial velocity versus x-location, measured in the ET-coordinate system, for the 704 cubic inch debris shape. The streamwise x-location of Reinforced-Carbon-Carbon (RCC) panel number eight is about x = 1800 inches, as designated by the dashed line labeled as the point of impact. This plot shows the effect of changing the debris-material density (and thus its mass). Two trajectories are drawn for each density (except the 5.0 lbs/ft^3 density case), each representing a different initial condition. The velocity at x=1800 inches is relatively independent of the initial condition, but strongly dependent on the density. The results clearly show that the relative axial velocity increases as the material density decreases.

An example of one Cart3D trajectory which closely resembled the strike location seen in the STS-107 film is shown in figure 17. This is the 1450 cubic inch piece of debris. It strikes the left-wing leading edge of the Orbiter on RCC panel number eight. The 6-DOF calculations show that this debris strikes the wing with a relative velocity of nearly 950 feet/sec. The elapsed time from the release of the debris to the impact on the wing is less than 0.15 seconds. During this time, the velocity of the vehicle increases by less than 10 feet/sec, thus the neglect of the vehicle acceleration introduces an error on the order of only one percent.

The analysis of the debris as seen on the launch video estimates that the foam is traveling between 775 and 820 feet/sec. The nominal density of the foam used to build the bipod ramps is 2.4 lbs/ft^3. As seen in figure 16, the CFD 6-DOF results predict much higher impact velocities than the video analysis for the 704 cubic inch piece. This result indicates that the debris would have to be significantly larger or of a higher density. In large part due to these CFD results, the CAIB determined that the debris was most likely larger than the

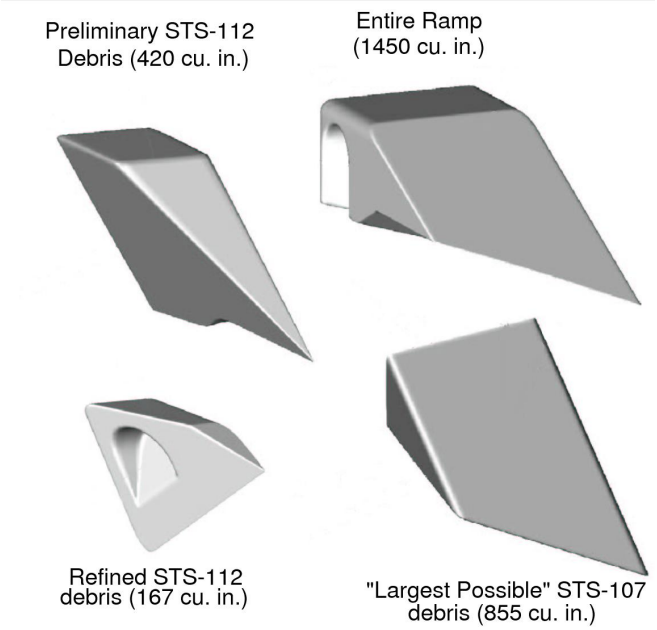


Figure 15. Four of the different debris shapes.

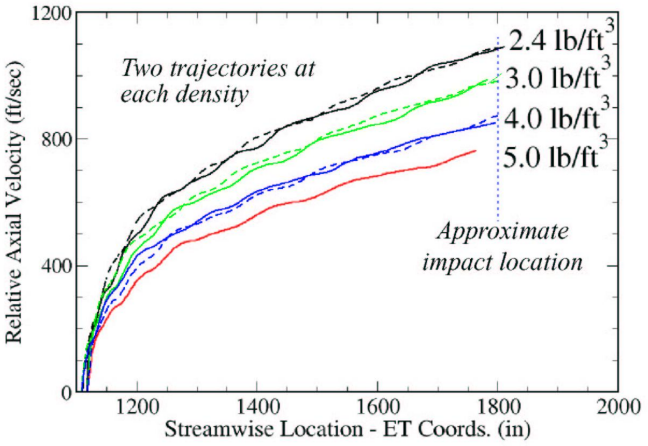


Figure 16. Axial velocities for debris pieces with volume of 704 cubic inches and different foam densities.

855 cubic inch piece. It was thus decided to use a 1200 cubic inch foam piece during the foam-firing tests into actual flight RCC panels. These tests ultimately proved that it was possible for a piece of foam to create a massive hole in an RCC panel.[1]

The effects of the debris on the surface pressures of the vehicle were estimated by subtracting the steady-state solution surface pressures from those computed during an unsteady trajectory Cart3D computation. This analysis shows that the Orbiter leading-edge pressure is lowered by approximately 0.4 psi just before the debris impact. This is shown in figure 18 which plots color contours of the difference in pressure on the vehicle surfaces at an instant in time when the debris is approaching the Orbiter wing leading edge. Red and yellow indicate increased pressures and cyan and blue indicate lowered local pressure. White or gray regions indicate small or no change in pressure. The lowered local wing-surface pressure is caused by the wake of the debris piece that precedes the debris as it travels past a fixed point on the Orbiter wing. Just upstream of this is a higher local pressure region that is caused by the shock formed upstream of the debris piece. This change in local surface pressure may help explain the anomalous accelerations measured on the left-wing outboard elevon accelerometer, which were recorded during the ascent of STS-107 immediately after the debris impact event.[8]

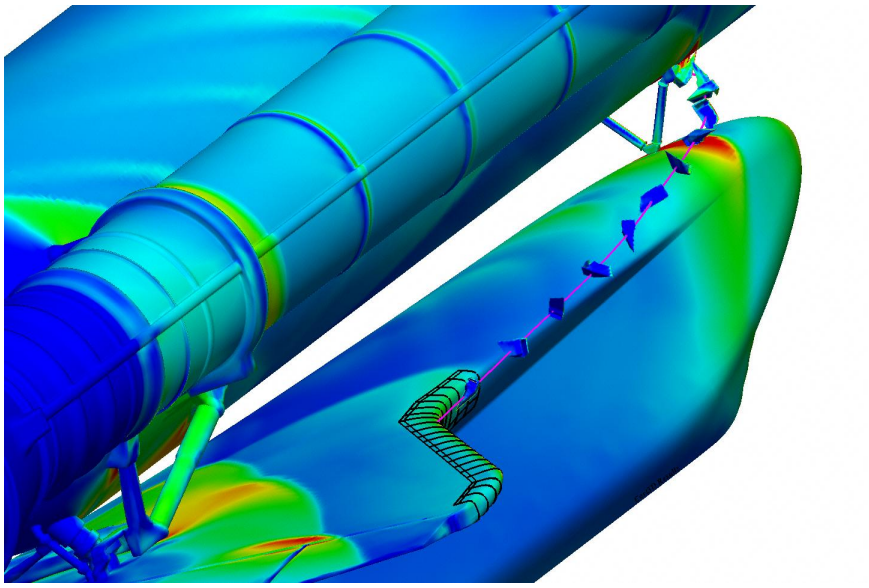


Figure 17. Cart3D 6-DOF debris trajectory.

VIII. Conclusion

Steady-state computations of the flow field around the Space Shuttle Launch Vehicle during ascent have been computed with the Overflow and Cart3D programs. These results have been utilized for simplified ballistic debris-trajectory computations, and were used to evaluate the air loads on the left bipod ramp. The loads computed by the Overflow code were consistently less than the design requirement loads, and indicate that air loads alone did not cause the bipod ramp to separate from the vehicle. Time-accurate 6-DOF moving-body simulations of the bipod-ramp foam debris have been computed with the Cart3D and Overflow-D codes. These simulations helped to define the impact velocity and foam size for the testing done under the direction of the CAIB in June of 2003. This testing subsequently showed that is was possible for a piece of foam debris to cause massive damage to the Shuttle Orbiter wing RCC panels and T-seals.

Acknowledgments

This work is dedicated to Astronaut Kalpana Chawla, who perished aboard STS-107. Before she became an astronaut, Kalpana worked as our colleague at NASA Ames on CFD research in the areas of powered lift, parallel computing, aerodynamic optimization, and multi-body aerodynamics. She was a good friend

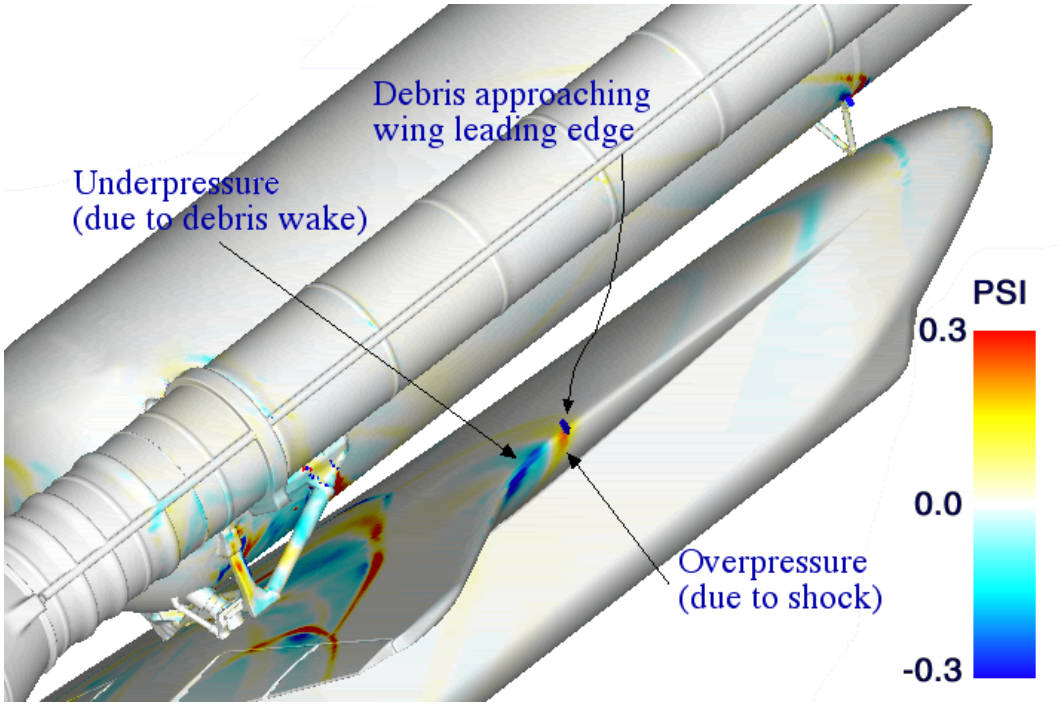


Figure 18. Delta pressure on the vehicle surface caused by debris as computed by Cart3D.

and will be missed.

The authors would like to acknowledge the excellent staff and world-class facilities of the NASA Advanced Supercomputer (NAS) facility at Ames Research Center, which provided us with over 400,000 hours of CPU time. Thanks also goes to the Department of Defense High-Performance-Computing Modernization Office for providing 40,000 hours of dedicated CPU time during the first few weeks of the investigation.

References

[1] *Columbia Accident Investigation Board Report Vol. 1*, U.S. Government Printing Office, Washington, DC, Aug. 2003.

[2] Kandula, M. and Buning, P. G., "Implementation of LU-SGS Algorithm and Roe Upwinding Scheme in OVERFLOW Thin-Layer Navier-Stokes Code," AIAA Paper 94-2357, AIAA 25th Fluid Dynamics Conference, Colorado Springs, CO, June 1994.

[3] Jespersen, D. C., Pulliam, T. H., and Buning, P. G., "Recent Enhancements to OVERFLOW," AIAA Paper 97-0644, Jan. 1997.

[4] Meakin, R., "Automatic Off-Body Grid Generation for Domains of Arbitrary Size," AIAA-2001-2536, 15th AIAA Computational Fluid Dynamics Conf., June 2001, Anaheim, CA.

[5] Meakin, R., "Adaptive Spatial Partitioning and Refinement for Overset Structured Grids," Comput. Methods Appl. Mech. Engrg., Vol. 189, pp. 1077-1117, 2000.

[6] Aftosmis, M. M., Berger, M. J., and Melton, J. E., "Robust and Efficient Cartesian Mesh Generation for Component-Based Geometry," *AIAA Journal*, Vol. 36, No. 6, pp. 952–960, June 1998, also AIAA Paper 97-0196, Jan. 1997.

[7] Aftosmis, M.J, Berger M.J., and Adomavicius, G., "A Parallel Multilevel Method for Adaptively Refined Cartesian Grids with Embedded Boundaries," AIAA Paper 2000-0808, Jan. 2000.

[8] *Columbia Accident Investigation Board Report Vol. 2*, Appendix D.8, pp. 235–271, U.S. Government Printing Office, Washington, DC, Oct. 2003.

[9] Steger, J., Dougherty, C., and Benek, J., "A Chimera Grid Scheme," Advances in Grid Generation, K. N. Ghia and U. Ghia, eds., ASME FED-Vol 5., June 1983.

[10] Buning, P. G., Chiu, I. T., Obayashi, S., Rizk, Y. M., and Steger, J. L., "Numerical Simulation of the Integrated Space Shuttle Vehicle in Ascent," AIAA Paper 88-4359-CP, 1988.

[11] Pearce, D. G., Stanley, S. A., Martin, F. W., Gomez, R. J., Le Beau, G. J., Buning, P. G., Chan, W. M., Chiu, I. T., Wulf, A. and Akdag, V., "Development of a Large Scale Chimera Grid System for the Space Shuttle Launch Vehicle," AIAA Paper 93-0533, 1993.

[12] Slotnick, J. P., Kandula, M., Buning, P. G., and Martin, F. W., "Numerical Simulation of the Space Shuttle Launch Vehicle Flowfield with Real Gas Solid Rocket Motor Plume Effects," AIAA Paper 93-0521, 1993.

[13] Slotnick, J. P., Kandula, M. and Buning, P. G., "Navier-Stokes Simulation of the Space Shuttle Launch Vehicle Flight Transonic Flowfield Using a Large Scale Chimera Grid System," AIAA Paper 94-1860, *Proceedings of the 12th AIAA Applied Aerodynamics Conference,* Colorado Springs, Colorado, 1994.

[14] Gomez, R. J. and Ma, E. C., "Validation of a Large Scale Chimera Grid System for the Space Shuttle Launch Vehicle," AIAA Paper 94-1859, *Proceedings of the AIAA 12th Applied Aerodynamics Conference,* Colorado Springs, Colorado, 1994.

[15] Martin, F. W., Labbe, S. G., Wey, T. C., and Pearce, D. G., "Space Shuttle Launch Vehicle Wind Tunnel and Flight Aerodynamic Environments," AIAA Paper 94-1861, *Proceedings of the AIAA 12th Applied Aerodynamics Conference,* Colorado Springs, Colorado, 1994.

[16] Taft, J. R., "Achieving 60 GFLOP/s on the Production CFD Code OVERFLOW-MLP," *Parallel Computing*, Vol. 27, No. 4, pp. 521-536, 2001.

[17] Marshall, D.D., Aftosmis, M.J., and Ruffin, S.M., "Study of Parallelization Enhancements For A Cartesian Grid Solver." *Proceedings of the International conference on Parallel CFD 2002*, Kansai Science City, Japan, May 2002.

[18] Aftosmis, M.J., Berger, M.J., Murman, S.M., "Applications of Space-Filling Curves to Cartesian Methods For CFD," AIAA Paper 2004-1232, Jan. 2004.

[19] Murman, S. M., Aftosmis, M.J., and Berger M.J., "Numerical Simulation of Rolling-Airframes Using a Multi-Level Cartesian Method," AIAA Paper 2002-2798, June 2002.

[20] Murman, S.M., Aftosmis, M.J., and Berger, M.J., "Implicit Approaches For Moving Boundaries in a 3-D Cartesian Method," AIAA Paper 2003-1119, Jan. 2003.

[21] Murman, S.M., Aftosmis, M.J., and Berger, M.J., "Simulations of 6-DOF Motion With a Cartesian Method," AIAA 2003-1246, Jan. 2003.

[22] Rogers, S. E., Roth, K., Nash, S. M., Baker, M. D., Slotnick, J. P., Whitlock, M., and Cao, H. V., "Advances in Overset CFD Processes Applied to Subsonic High-Lift Aircraft," AIAA Paper 2000-4216, Aug. 2000.

[23] Chan, W. M., "The Overgrid Interface for Computational Simulations on Overset Grids," AIAA Paper 2002-3188, June 2002.

[24] Rogers, S. E., Suhs, N. E., and Dietz, W. E. "PEGASUS 5: An Automated Pre-processor for Overset-Grid CFD," *AIAA Journal*, Vol. 41, No. 6, June 2003, pp. 1037–1045.

[25] Marroquin, J. and Lemoine, P., "Results of Wind Tunnel Tests of an ASRM Configured 0.03 Scale Space Shuttle Integrated Vehicle Model (47-OTS) in the AEDC 16-foot Transonic Wind Tunnel (IA613A)," NASA Center for Aerospace Information (CASI), NASA-CR-185696, 1992.